

<https://doi.org/10.15407/ujpe67.6.383>

M. AYGUN

Department of Physics, Bitlis Eren University  
(Beş Minare Mah., Rahva Yerleskesi, 13000 Bitlis, Turkey; e-mail: murata.25@gmail.com)

## ANALYSIS OF ELASTIC SCATTERING CROSS-SECTIONS OF CARBON ISOTOPES ( $^{10-16}\text{C}$ ) USING DIFFERENT NUCLEON-NUCLEON INTERACTIONS

---

*In this study, the comparative analysis of different nucleon-nucleon interactions is carried out in the framework of the optical model. The real potential is obtained using the double folding model for eight different nucleon-nucleon interactions which consist of B, G1, G2, SL, R3Y(HS), R3Y(Z), R3Y(W), and R3Y(L1). The results are compared with M3Y nucleon-nucleon results, as well as the experimental data in order to perform a comparative study. The similarities and differences of the nucleon-nucleon interactions are discussed, and alternative nucleon-nucleon interactions are proposed for the analysis of carbon isotopes ( $^{10-16}\text{C}$ ).*

*Keywords:* nucleon-nucleon interaction, relativistic mean field, optical model, double folding model.

### 1. Introduction

The nucleon-nucleon ( $NN$ ) interaction plays a significant role for the nuclear force and nuclear structure and is a very important parameter in the theoretical analysis of any nuclear reaction. In this manner, various  $NN$  interactions have been developed. For example, Bertsch *et al.* [1] have proposed a Yukawa-type  $NN$  interaction. Greenless *et al.* [2] have shown a Gauss-type  $NN$  interaction. Ball *et al.* [3] have reported on the  $NN$  interaction consisting of two Gauss-type terms. Satchler and Love [4] suggested a different  $NN$  interaction. Additionally, four different  $NN$  interactions such as R3Y (HS), R3Y (Z), R3Y (W), R3Y (L1) have been proposed under the relativistic mean field (RMF) theory [5,6]. The RMF theory is one of the microscopic approaches evaluated to obtain a solution to many-body problem. It assumes that nucleons interact through the meson exchange [7]. The  $NN$  interactions have been researched for radioactive decays [8], proton radioactivity [9], and

fusion reactions [10]. Finally, M3Y  $NN$  interaction which consists of three Yukawa-type  $NN$  interaction is well known in the literature [11].

In the present work, we aim to give acceptable and alternative  $NN$  interaction(s) for the analysis of the elastic scattering cross-sections of carbon isotopes ( $^{10-16}\text{C}$ ). For this, we examine the effects of different  $NN$  interactions on the analysis of elastic scattering cross-sections. In this context, we calculate the elastic scattering cross-sections of carbon isotopes ( $^{10-16}\text{C}$ ) with various target nuclei by using B, G1, G2, SL, R3Y(HS), R3Y(Z), R3Y(W), and R3Y(L1)  $NN$  interaction potentials, as well as M3Y  $NN$  interaction. We compare the theoretical results and the experimental data. Thus, we evaluate the similarities and differences of the  $NN$  interactions and report alternative  $NN$  interactions for the elastic scattering analysis of carbon isotopes ( $^{10-16}\text{C}$ ).

The study is organized as follows. In Section 2, the theoretical formalism used in the calculations is presented. In Section 3, the investigated  $NN$  interactions are summarized. In Section 4, the results

are discussed. Finally, the conclusions are shown in Section 5.

## 2. Theoretical Formalism

The total potential ( $V_{\text{Total}}$ ) defining the studied systems can be given in the following form:

$$V_{\text{Total}}(r) = V_{\text{Coulomb}}(r) + V_{\text{Nuclear}}(r). \quad (1)$$

The  $V_{\text{Coulomb}}(r)$  potential [4] is accepted as

$$V_{\text{C}}(r) = \frac{1}{4\pi\epsilon_0} \frac{Z_P Z_T e^2}{r}, \quad r \geq R_c, \quad (2)$$

$$= \frac{1}{4\pi\epsilon_0} \frac{Z_P Z_T e^2}{2R_c} \left( 3 - \frac{r^2}{R_c^2} \right), \quad r < R_c, \quad (3)$$

where  $R_c$  is the Coulomb radius,  $Z_P(Z_T)$  and  $A_P(A_T)$  are the atomic and mass numbers of projectile (target), respectively. The  $V_{\text{Nuclear}}(r)$  potential is obtained within the optical model that consists of the real and imaginary parts. In this way, the real potential is produced with the help of the double folding potential parameterized by

$$V(\mathbf{r}) = N_R \int d\mathbf{r}_1 \int d\mathbf{r}_2 \rho_P(\mathbf{r}_1) \rho_T(\mathbf{r}_2) \times \nu_{NN}[\mathbf{r} - (\mathbf{r}_1 - \mathbf{r}_2)], \quad (4)$$

where  $N_R$  is the renormalization factor,  $\rho_{P(T)}(\mathbf{r}_{1(2)})$  is the density of projectile(target) and  $\nu_{NN}$  is

*Table 1. The parameters of two-parameter Fermi (2pF) density for the  $^{10-16}\text{C}$ ,  $^{27}\text{Al}$ ,  $^{28}\text{Si}$ ,  $^{40}\text{Ca}$ ,  $^{90}\text{Zr}$ ,  $^{138}\text{Ba}$  and  $^{238}\text{Pb}$  nuclei*

Nucleus	$c$ (fm)	$z$ (fm)	$\rho_0$ ( $\text{fm}^{-3}$ )	Ref.
$^{10}\text{C}$	1.8542	0.446608	0.238136	[12]
$^{11}\text{C}$	1.93441	0.452909	0.235422	[12]
$^{12}\text{C}$	2.01294	0.45901	0.232115	[12]
$^{13}\text{C}$	2.08983	0.464917	0.228446	[12]
$^{14}\text{C}$	2.16511	0.470631	0.224577	[12]
$^{15}\text{C}$	2.23879	0.476157	0.220627	[12]
$^{16}\text{C}$	2.31091	0.481497	0.216675	[12]
$^{14}\text{N}$	2.20079	0.475549	0.214639	[12]
$^{27}\text{Al}$	2.84	0.569	0.2015	[13]
$^{28}\text{Si}$	3.15	0.475	0.175	[14]
$^{40}\text{Ca}$	3.60	0.523	0.169	[14]
$^{90}\text{Zr}$	4.90	0.515	0.165	[14]
$^{138}\text{Ba}$	5.60	0.540	0.171930	[15]
$^{208}\text{Pb}$	6.62	0.551	0.1600	[13]

nucleon-nucleon interaction. For all the projectile and target nuclei, we have used two-parameter Fermi (2pF) density distribution

$$\rho(r) = \frac{\rho_0}{1 + \exp\left(\frac{r-c}{z}\right)}, \quad (5)$$

where  $\rho_0$ ,  $c$  and  $z$  values are listed in Table 1. The imaginary part is assumed as the Woods-Saxon potential given by

$$W(r) = -iW_0(1+e^x)^{-1}, \quad e^x = \frac{r - r_w (A_P^{1/3} + A_T^{1/3})}{a_w}, \quad (6)$$

where  $W_0$ ,  $r_w$  and  $a_w$  are the depth, radius, and diffuseness parameters. The codes DFPOt [16] and FRESco [17] are used in the double folding model and the optical model calculations, respectively.

## 3. Microscopic NN Interactions

### 3.1. Bertsch (B) interaction

The B interaction [1] is

$$\nu_{NN}^{\text{B}}(r) = -2105.1 \frac{e^{-4r}}{4r} + 653.6 \frac{e^{-2.5r}}{2.5r} + 1.3 \frac{e^{-0.707r}}{0.707r} + J_{00}(E)\delta(r), \quad (7)$$

where  $J_{00}(E)$ , the exchange term, is shown by

$$J_{00}(E) = -276 \left[ 1 - 0.005 \frac{E_{\text{Lab}}}{A_p} \right] \text{MeV fm}^3, \quad (8)$$

where  $E_{\text{Lab}}$  is the incident energy.

### 3.2. Gaussian 1 (G1) interaction

The G1 interaction, which is introduced by Greenless *et al.* [2], can be given as

$$\nu_{NN}^{\text{G1}}(r) = -22.332 e^{(-0.46r^2)} + J_{00}(E)\delta(r). \quad (9)$$

### 3.3. Gaussian 2 (G2) interaction

The G2 interaction [3] takes the following form:

$$\nu_{NN}^{\text{G2}}(r) = -5.447 e^{(-0.292r^2)} - 12.448 e^{(-0.415r^2)} + J_{00}(E)\delta(r). \quad (10)$$

### 3.4. Satchler and Love (SL) interaction

The SL interaction [4] can be identified by

$$\nu_{NN}^{\text{SL}}(r) = 6315 \frac{e^{-4r}}{4r} - 1961 \frac{e^{-2.5r}}{2.5r} - 81\delta(r). \quad (11)$$

### 3.5. R3Y (HS) interaction

The R3Y (HS) interaction [5] can be written as

$$\nu_{NN}^{\text{R3Y(HS)}}(r) = 11957 \frac{e^{-3.97r}}{4r} + 4099 \frac{e^{-3.90r}}{4r} - 6883 \frac{e^{-2.64r}}{4r} + J_{00}(E)\delta(r). \quad (12)$$

### 3.6. R3Y (Z) interaction

The R3Y (Z) interaction [6] can be presented by

$$\nu_{NN}^{\text{R3Y(Z)}}(r) = 12009 \frac{e^{-3.96r}}{4r} + 7446 \frac{e^{-3.87r}}{4r} - 7862 \frac{e^{-2.80r}}{4r} + J_{00}(E)\delta(r). \quad (13)$$

### 3.7. R3Y (W) interaction

The R3Y (W) interaction [6] becomes

$$\nu_{NN}^{\text{R3Y(W)}}(r) = 8551 \frac{e^{-3.97r}}{4r} - 5750 \frac{e^{-2.79r}}{4r} + J_{00}(E)\delta(r). \quad (14)$$

### 3.8. R3Y (L1) NN interaction

The R3Y (L1) interaction [6] can be given as

$$\nu_{NN}^{\text{R3Y(L1)}}(r) = 9968 \frac{e^{-3.97r}}{4r} - 6661 \frac{e^{-2.79r}}{4r} + J_{00}(E)\delta(r). \quad (15)$$

### 3.9. M3Y interaction

In order to make a comparative study, we perform the theoretical calculations for the M3Y NN interaction. Thus, we can discuss the similarities and differences of the investigated NN interactions. The M3Y interaction that is used in the analysis of numerous nuclear reactions is one of the most popular interaction potentials [18–21]. The M3Y, which is produced with G-matrix elements under Reid–Elliott soft core NN interaction [22], consists of the sum of three Yukawa potentials with ranges 0.25 fm for a medium-range attractive part and 0.4 fm for a short-range repulsive part. Thus, the M3Y interaction can be written as [11]

$$\nu_{NN}^{\text{M3Y}}(r) = 7999 \frac{e^{-4r}}{4r} - 2134 \frac{e^{-2.5r}}{2.5r} + J_{00}(E)\delta(r). \quad (16)$$

## 4. Results and Discussion

We have examined the effect of eight different NN interaction potentials on the elastic scattering cross-sections of carbon isotopes ( $^{10-16}\text{C}$ ). We have presented the changes with the distance of the NN interactions without the  $J_{00}(E)$  term in Fig. 1. To make a comparative research, we have also plotted the M3Y NN interaction.

In our study, we have first examined the variations with the distance of real potentials calculated for different interactions. In this context, we have comparatively plotted the real potentials for  $^{11}\text{C}$ ,  $^{12}\text{C}$  and  $^{15}\text{C}$  projectiles scattered from the same target ( $^{208}\text{Pb}$ ) in Fig. 2. We have observed that the behavior of the real potentials is the same for all three reactions. In this regard, the real potentials for the other interactions show an attractive behavior similar to each other, while the behavior of the real potential for the R3Y(Z) interaction is repulsive.

The NN interactions have been calculated by means of the code FORTRAN developed by us. The optical potential has been determined in the scope of the real potential produced by using the NN interactions and the code DFPOT together with the imaginary part based on the Woods–Saxon potential. The normalization constant ( $N_R$ ) is used in the double folding calculations to increase the harmony of the experiment and theory. Its normally default value is 1.0, and the deviation from this value may be due to either uncertainty or peculiarity of the data or the fitting process. We have assumed as  $N_R = 1.0$  for all the calculations in our study in order to eliminate the effect of the  $N_R$  value on the theoretical results. The depth ( $W_0$ ) in MeV, radius and diffuseness parameters ( $r_w$  and  $a_w$ ) in fm of the imaginary potential have been released in order to obtain optimum results with the experimental data. In this way, the  $r_w$  value is found by varying, at 0.1 and 0.01 fm, the interval at fixed  $W_0$  and  $a_w$ . Then the  $a_w$  value is determined by varying, at 0.1 and 0.01 fm, the interval at fixed  $W_0$  and  $r_w$ . Finally, the  $W_0$  value is acquired for fixed  $r_w$  and  $a_w$ . Thus, the values of  $W_0$ ,  $r_w$ , and  $a_w$  parameters are given in Tables 2, 3 and 4, respectively.

In this research, the elastic scattering cross-sections of six different carbon isotopes ( $^{10-16}\text{C}$ ) by different target nuclei have been calculated for nine different NN interactions. First, the elastic cross-section of

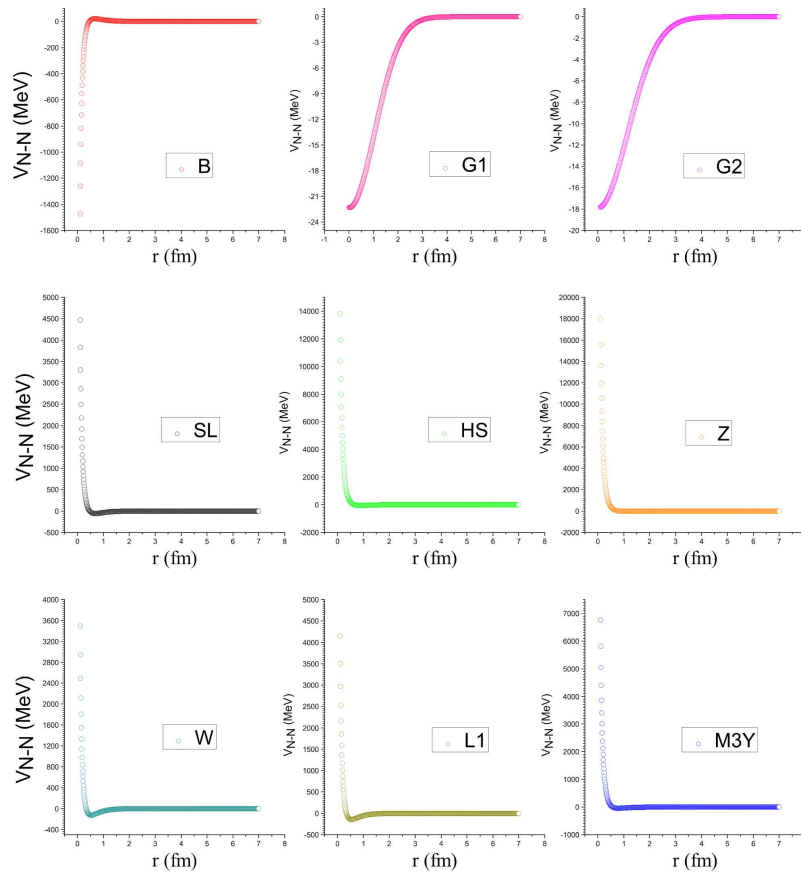


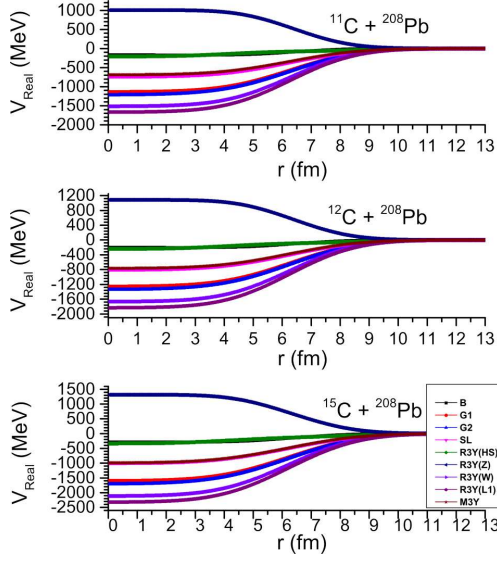
Fig. 1. A comparison of B, G1, G2, SL, R3Y (HS), R3Y (Z), R3Y (W), R3Y (L1), and M3Y effective NN interactions as a function of the distance

Table 2. The  $W_0$  values (in MeV) obtained for B, G1, G2, SL, R3Y(HS), R3Y(Z), R3Y(W), R3Y(L1), and M3Y interactions

Reaction	B	G1	G2	SL	HS	Z	W	L1	M3Y
$^{10}\text{C} + ^{27}\text{Al}$	18.5	22.0	29.0	19.5	10.0	9.70	19.5	15.5	25.5
$^{11}\text{C} + ^{14}\text{N}$	24.0	32.0	24.0	25.0	25.0	16.0	31.0	33.0	33.0
$^{11}\text{C} + ^{208}\text{Pb}$	10.7	51.0	51.0	51.0	41.0	51.0	51.0	61.0	51.0
$^{12}\text{C} + ^{28}\text{Si}$	11.5	11.5	8.00	11.5	11.5	10.5	10.5	11.5	10.0
$^{12}\text{C} + ^{90}\text{Zr}$	13.0	15.0	15.0	7.0	7.0	10.0	13.0	9.0	7.0
$^{12}\text{C} + ^{208}\text{Pb}$	32.0	32.0	90.0	15.0	12.0	17.0	65.0	75.0	15.0
$^{13}\text{C} + ^{12}\text{C}$	62.0	62.0	72.0	13.0	10.0	13.0	18.0	13.0	13.0
$^{13}\text{C} + ^{28}\text{Si}$	15.0	15.0	15.0	15.0	15.0	15.5	15.0	13.0	15.0
$^{14}\text{C} + ^{13}\text{C}$	4.5	9.5	9.5	28.0	14.2	25.5	22.0	22.0	15.5
$^{14}\text{C} + ^{40}\text{Ca}$	15.0	10.0	10.0	10.0	10.0	16.0	10.0	10.0	10.0
$^{14}\text{C} + ^{138}\text{Ba}$	16.0	16.0	20.0	20.0	11.0	16.0	21.0	21.0	11.0
$^{15}\text{C} + ^{208}\text{Pb}$	62.0	62.0	62.0	62.0	62.0	62.0	62.0	62.0	62.0
$^{16}\text{C} + ^{12}\text{C}$	14.6	24.0	24.0	21.0	24.0	30.0	24.0	25.0	20.0

Table 3. Same as Table 2, but for  $r_w$  values

Reaction	B	G1	G2	SL	HS	Z	W	L1	M3Y
$^{10}\text{C} + ^{27}\text{Al}$	1.40	1.40	1.45	1.40	1.40	1.40	1.40	1.30	1.25
$^{11}\text{C} + ^{14}\text{N}$	1.40	1.40	1.40	1.40	1.40	1.40	1.40	1.40	1.40
$^{11}\text{C} + ^{208}\text{Pb}$	1.35	1.32	1.32	1.31	1.32	1.31	1.32	1.32	1.32
$^{12}\text{C} + ^{28}\text{Si}$	1.40	1.40	1.45	1.32	1.28	1.40	1.30	1.35	1.27
$^{12}\text{C} + ^{90}\text{Zr}$	1.40	1.37	1.37	1.36	1.35	1.36	1.39	1.36	1.36
$^{12}\text{C} + ^{208}\text{Pb}$	1.28	1.28	1.28	1.28	1.28	1.28	1.29	1.28	1.28
$^{13}\text{C} + ^{12}\text{C}$	1.00	1.00	1.00	1.28	1.28	1.33	1.23	1.28	1.28
$^{13}\text{C} + ^{28}\text{Si}$	1.42	1.42	1.42	1.42	1.42	1.42	1.42	1.42	1.42
$^{14}\text{C} + ^{13}\text{C}$	1.40	1.40	1.38	1.10	1.10	1.10	1.10	1.10	1.10
$^{14}\text{C} + ^{40}\text{Ca}$	1.38	1.41	1.41	1.31	1.31	1.41	1.41	1.41	1.31
$^{14}\text{C} + ^{138}\text{Ba}$	1.30	1.30	1.33	1.23	1.24	1.27	1.24	1.24	1.24
$^{15}\text{C} + ^{208}\text{Pb}$	1.47	1.47	1.47	1.48	1.48	1.48	1.48	1.47	1.48
$^{16}\text{C} + ^{12}\text{C}$	1.40	1.40	1.43	1.43	1.33	1.40	1.41	1.40	1.40



**Fig. 2.** A comparison as a function of the distance of the real potentials calculated for  $^{11}\text{C} + ^{208}\text{Pb}$ ,  $^{12}\text{C} + ^{208}\text{Pb}$  and  $^{15}\text{C} + ^{208}\text{Pb}$  reactions by using the B, G1, G2, SL, R3Y (HS), R3Y (Z), R3Y (W), R3Y (L1), and M3Y effective  $NN$  interactions

$^{10}\text{C} + ^{27}\text{Al}$  reaction has been calculated at 29.1 MeV and has been compared with the data in Fig. 3. The result with R3Y (L1)  $NN$  interaction has exhibited a quite different behavior from the results with other  $NN$  interactions. In addition, it has been noticed that R3Y(HS) has provided better results than the other  $NN$  interactions except for M3Y.

**Table 4.** Same as Table 2, but for  $a_w$  values

Reaction	B	G1	G2	SL	HS	Z	W	L1	M3Y
$^{10}\text{C} + ^{27}\text{Al}$	0.80	0.50	0.44	0.59	0.55	0.82	0.45	0.55	0.48
$^{11}\text{C} + ^{14}\text{N}$	0.72	0.65	0.52	0.58	0.58	0.58	0.58	0.58	0.62
$^{11}\text{C} + ^{208}\text{Pb}$	0.58	0.30	0.30	0.30	0.30	0.30	0.30	0.30	0.30
$^{12}\text{C} + ^{28}\text{Si}$	0.93	0.63	0.43	0.73	0.63	0.83	0.58	0.60	0.63
$^{12}\text{C} + ^{90}\text{Zr}$	0.86	0.40	0.40	0.40	0.40	0.90	0.40	0.40	0.40
$^{12}\text{C} + ^{208}\text{Pb}$	0.80	0.40	0.40	0.40	0.40	0.90	0.30	0.40	0.40
$^{13}\text{C} + ^{12}\text{C}$	0.70	0.65	0.65	0.60	0.50	0.70	0.50	0.50	0.60
$^{13}\text{C} + ^{28}\text{Si}$	0.90	0.78	0.70	0.80	0.80	0.82	0.80	0.78	0.80
$^{14}\text{C} + ^{13}\text{C}$	0.80	0.60	0.50	0.90	0.90	0.90	0.90	0.90	0.90
$^{14}\text{C} + ^{40}\text{Ca}$	0.90	0.37	0.37	0.45	0.52	0.73	0.49	0.40	0.47
$^{14}\text{C} + ^{138}\text{Ba}$	0.90	0.50	0.40	0.85	0.77	0.80	0.55	0.55	0.75
$^{15}\text{C} + ^{208}\text{Pb}$	0.98	0.98	0.98	0.98	0.98	0.98	0.98	0.98	0.98
$^{16}\text{C} + ^{12}\text{C}$	0.43	0.37	0.37	0.32	0.32	0.42	0.41	0.41	0.37

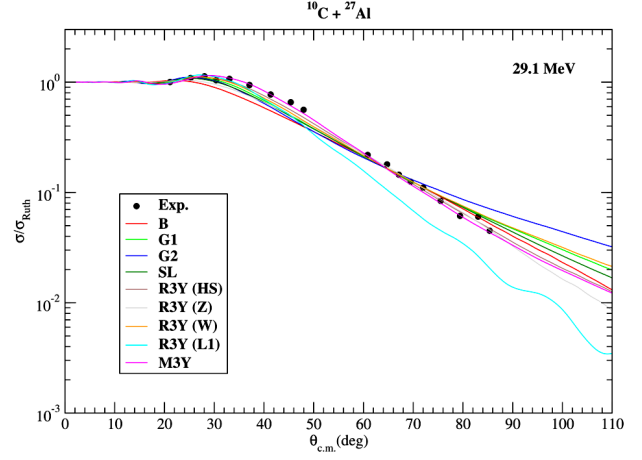


**Fig. 3.** The elastic scattering cross-sections of  $^{10}\text{C} + ^{27}\text{Al}$  reaction calculated using the B, G1, G2, SL, R3Y (HS), R3Y (Z), R3Y (W), R3Y (L1), and M3Y effective  $NN$  interactions at 29.1 MeV [23]

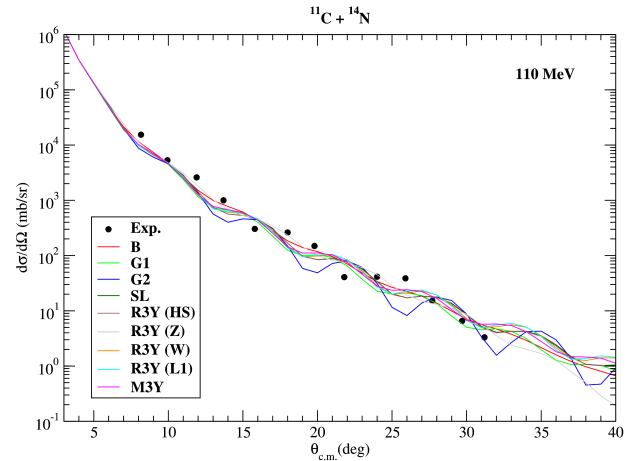


**Fig. 4.** Same as Fig. 3, but for  $^{11}\text{C} + ^{14}\text{N}$  at 110 MeV [23]

For  $^{11}\text{C}$  isotope, the scattering cross-sections of  $^{11}\text{C} + ^{14}\text{N}$  (at 110 MeV) and  $^{11}\text{C} + ^{208}\text{Pb}$  (at 226 MeV) systems have been obtained. The theoretical results and the data have been compared in Figs. 4 and 5, respectively. It is seen that the results with G2 for  $^{11}\text{C} + ^{14}\text{N}$  have slightly higher amplitudes compared to the results with other  $NN$  interactions. However, it is observed that the results for  $^{11}\text{C} + ^{208}\text{Pb}$  are different from each other in general. Additionally, it has been realized that the results with the R3Y(HS) and R3Y(Z) interactions are better than the other results.

For  $^{12}\text{C}$  isotope, the elastic cross-sections of  $^{12}\text{C} + ^{28}\text{Si}$  (at 49.3 MeV),  $^{12}\text{C} + ^{90}\text{Zr}$  (at 120 MeV) and

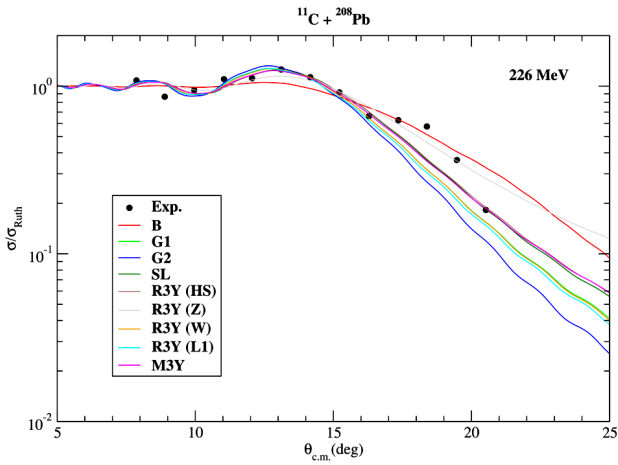


Fig. 5. Same as Fig. 3, but for  $^{11}\text{C}+^{208}\text{Pb}$  at 226 MeV [23]

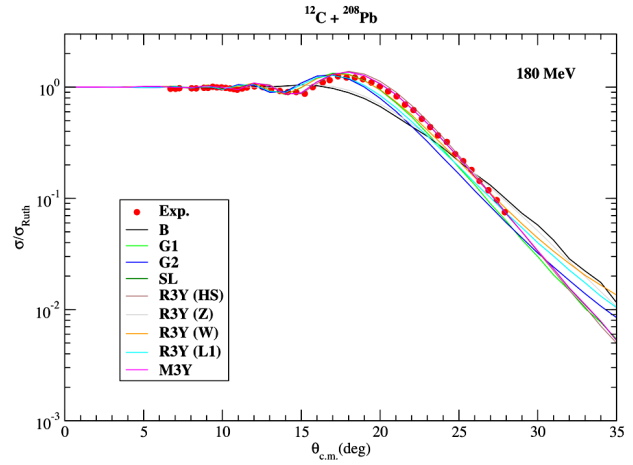


Fig. 8. Same as Fig. 3, but for  $^{12}\text{C}+^{208}\text{Pb}$  at 180 MeV [23]

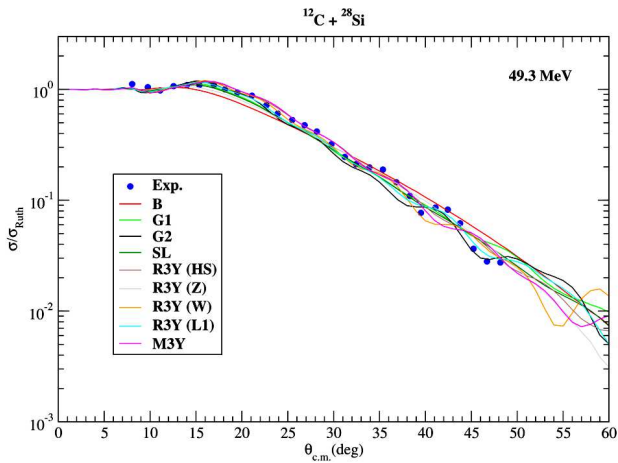


Fig. 6. Same as Fig. 3, but for  $^{12}\text{C}+^{28}\text{Si}$  at 49.3 MeV [23]

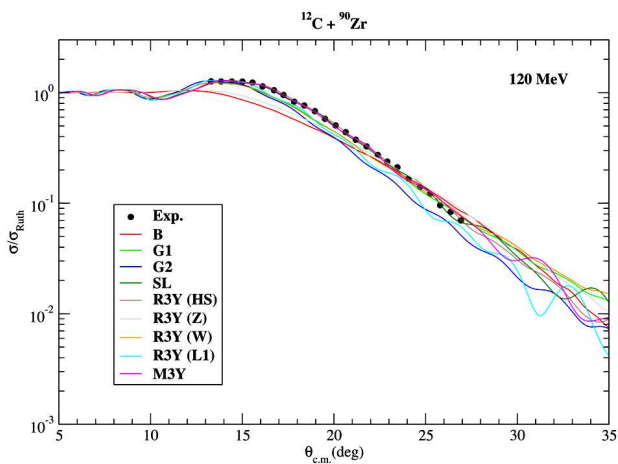


Fig. 7. Same as Fig. 3, but for  $^{12}\text{C}+^{90}\text{Zr}$  at 120 MeV [23]

$^{12}\text{C}+^{208}\text{Pb}$  (at 180 MeV) reactions as light, medium, and heavy target samples have been calculated and compared with the experimental data in Figs. 6, 7 and 8, respectively. The results for the  $^{12}\text{C}+^{28}\text{Si}$  reaction are close to each other. The results with the B, G1, G2, R3Y(Z), R3Y(W), and R3Y(L1)  $NN$  interactions for the  $^{12}\text{C}+^{90}\text{Zr}$  reaction are far from defining experimental data. On the other hand, the results with the SL and R3Y(HS) have been found to be compatible with each other and experimental data, as well as M3Y results. It is observed that the results with the SL, R3Y(HS), R3Y(W) are in agreement with the data, while the results with the B, G1, G2, R3Y(Z) and R3Y(L1)  $NN$  interactions for the  $^{12}\text{C}+^{208}\text{Pb}$  system could not describe the experimental data well. It has been realized that the results with SL and R3Y(HS)  $NN$  interactions are better than the other results.

For  $^{13}\text{C}$  isotope, the elastic scattering cross-sections of  $^{13}\text{C}+^{12}\text{C}$  (at 650 MeV) and  $^{13}\text{C}+^{28}\text{Si}$  (at 60 MeV) systems whose experimental data can be obtained from the literature have been calculated and compared with data in Figs. 9 and 10, respectively. It is observed that the results with different interaction potentials for both reactions have displayed a similar behavior generally. However, it has been recognized that the results based on R3Y(HS) interaction are in better agreement with the experimental data compared to the results with other  $NN$  interactions.

For  $^{14}\text{C}$  isotope, the scattering cross-sections of  $^{14}\text{C}+^{13}\text{C}$  (at 168 MeV),  $^{14}\text{C}+^{40}\text{Ca}$  (at 51 MeV) and  $^{14}\text{C}+^{138}\text{Ba}$  (at 64 MeV) reactions as light, medium,

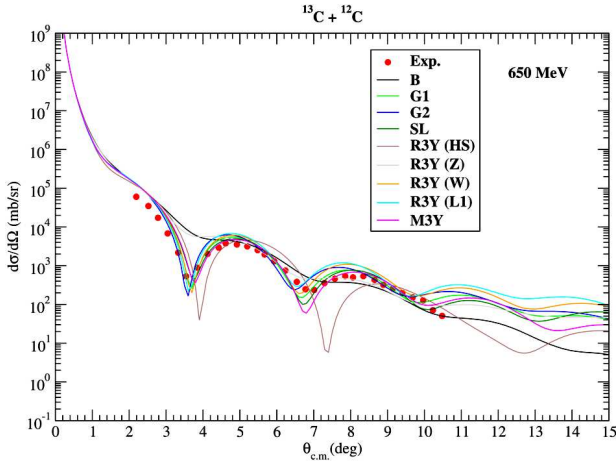


Fig. 9. Same as Fig. 3, but for  $^{13}\text{C}+^{12}\text{C}$  at 650 MeV [23]

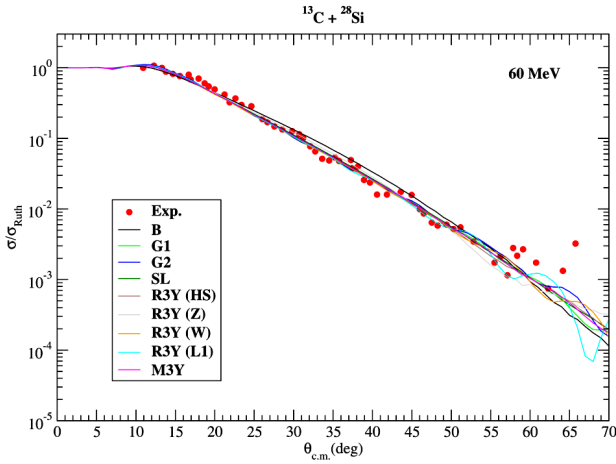


Fig. 10. Same as Fig. 3, but for  $^{13}\text{C}+^{28}\text{Si}$  at 60 MeV [23]

and heavy target samples have been obtained. The theoretical results have been compared with the experimental data in Figs. 11, 12 and 13, respectively. The results with the R3Y(HS)  $NN$  interaction are better than the results with the other interactions in general.

Then the elastic scattering cross-section of  $^{15}\text{C} + ^{208}\text{Pb}$  system has been calculated for nine various  $NN$  interactions at 65 MeV due to acquiring the experimental data for a single reaction of the  $^{15}\text{C}$  isotope in the literature. The theoretical results and the experimental data have been compared in Fig. 14. It is seen that the results by means of different  $NN$  interactions have displayed a similar behavior with each other and experimental data.

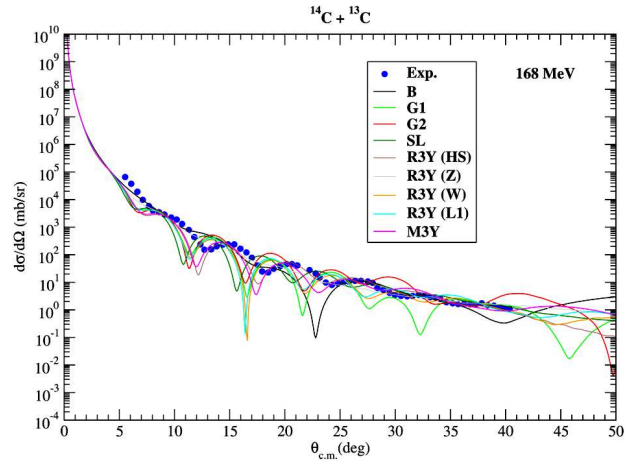


Fig. 11. Same as Fig. 3, but for  $^{14}\text{C}+^{13}\text{C}$  at 168 MeV [23]

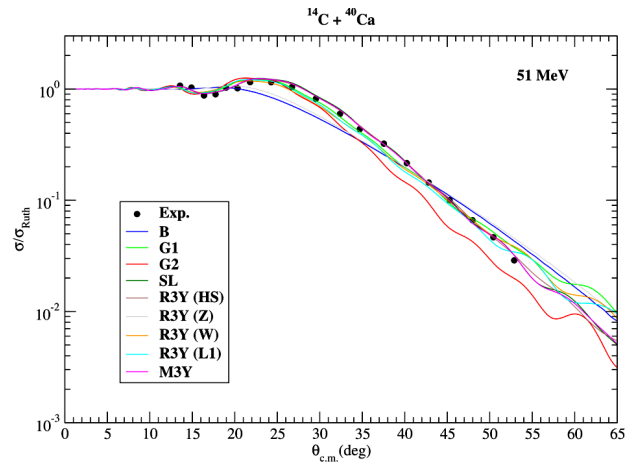


Fig. 12. Same as Fig. 3, but for  $^{14}\text{C}+^{40}\text{Ca}$  at 51 MeV [23]

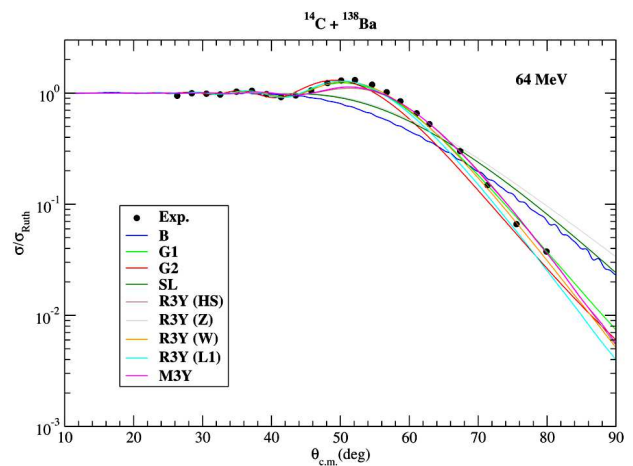


Fig. 13. Same as Fig. 3, but for  $^{14}\text{C}+^{138}\text{Ba}$  at 64 MeV [23]

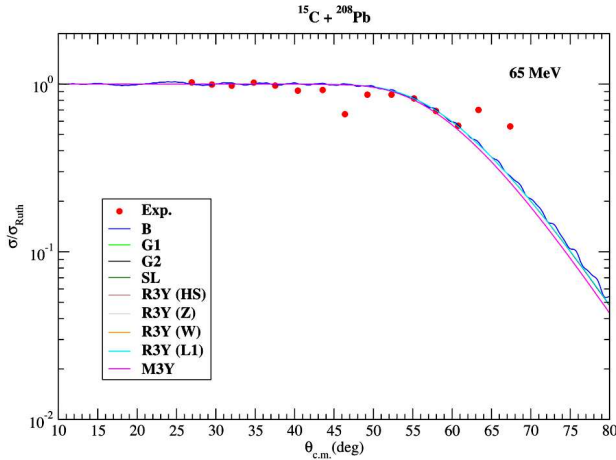


Fig. 14. Same as Fig. 3, but for  $^{15}\text{C} + ^{208}\text{Pb}$  at 65 MeV [24]

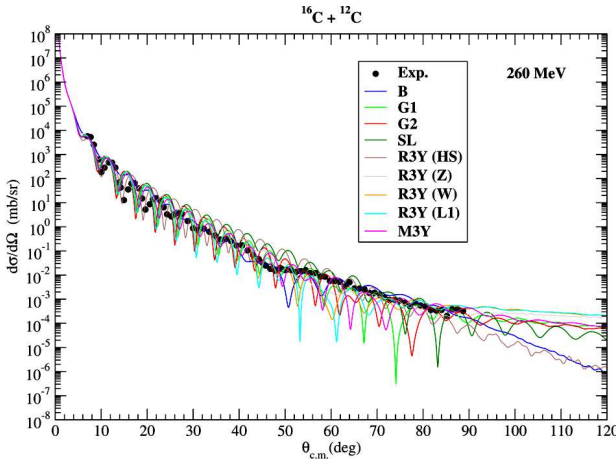


Fig. 15. Same as Fig. 3, but for  $^{16}\text{C} + ^{12}\text{C}$  at 260 MeV [23]

Finally, for only a single reaction similar to the  $^{15}\text{C}$  isotope, the elastic cross-section of  $^{16}\text{C} + ^{12}\text{C}$  system has been calculated at 260 MeV. The theoretical results have been compared with the experimental data in Fig. 15. It is seen that the result with the B  $NN$  interaction is better than the results with the other  $NN$  interactions.

The cross-section value is a useful parameter in producing an alternative  $NN$  interaction. In this context, we have showed the cross-section values for each  $NN$  interaction and each nuclear reaction in Table 5. We observe that the cross-sections are different from each other according to the differences of  $NN$  interactions. However, the results with the G1 and G2 have been generally observed to be close to each other. In addition, the results with the SL, R3Y (HS)

and M3Y interactions have been seen to be close to each other. From this point of view, it can be said that the SL and R3Y (HS) interactions are close to M3Y interaction.

We have calculated the  $\chi^2/N$  values for the results with all  $NN$  interactions and have listed the results in Table 6. It is seen that the  $\chi^2/N$  values are low for all the reactions except for  $^{13}\text{C} + ^{12}\text{C}$  and  $^{16}\text{C} + ^{12}\text{C}$  reactions. It can be also noted that the R3Y (HS) interaction has given the lowest  $\chi^2/N$

Table 5. The cross-sections (in mb) values for B, G1, G2, SL, R3Y(HS), R3Y(Z), R3Y(W), R3Y(L1), and M3Y interactions

Reaction	B	G1	G2	SL	HS	Z	W	L1	M3Y
$^{10}\text{C} + ^{27}\text{Al}$	1501	1117	1168	1202	1026	1311	1043	1042	891
$^{11}\text{C} + ^{14}\text{N}$	2065	2066	1774	1855	1854	1693	1924	1945	2011
$^{11}\text{C} + ^{208}\text{Pb}$	3258	3139	3165	3071	3072	3003	3142	3180	3116
$^{12}\text{C} + ^{28}\text{Si}$	2140	1700	1525	1786	1443	1930	1453	1577	1407
$^{12}\text{C} + ^{90}\text{Zr}$	3107	2297	2329	2091	2050	2857	2332	2198	2090
$^{12}\text{C} + ^{208}\text{Pb}$	3745	2879	3120	2690	2622	3616	2845	3066	2689
$^{13}\text{C} + ^{12}\text{C}$	1383	1351	1400	1335	1148	1462	1284	1286	1331
$^{13}\text{C} + ^{28}\text{Si}$	2476	2269	2135	2295	2300	2338	2307	2213	2300
$^{14}\text{C} + ^{13}\text{C}$	1531	1750	1636	1987	1639	1828	1855	1863	1690
$^{14}\text{C} + ^{40}\text{Ca}$	2236	1446	1500	1325	1376	2017	1573	1495	1344
$^{14}\text{C} + ^{138}\text{Ba}$	1859	1258	1276	1605	1346	1550	1242	1260	1327
$^{15}\text{C} + ^{208}\text{Pb}$	3043	3050	3050	3111	3111	3110	3111	3050	3111
$^{16}\text{C} + ^{12}\text{C}$	1632	1719	1793	1686	1504	1799	1792	1783	1674

Table 6. The  $\chi^2/N$  values calculated for B, G1, G2, SL, R3Y(HS), R3Y(Z), R3Y(W), R3Y(L1) and M3Y interactions

Reaction	B	G1	G2	SL	HS	Z	W	L1	M3Y
$^{10}\text{C} + ^{27}\text{Al}$	3.10	1.96	5.44	2.01	0.53	1.53	1.71	11.3	0.45
$^{11}\text{C} + ^{14}\text{N}$	26.6	27.9	37.2	33.6	32.7	26.2	36.2	36.4	33.0
$^{11}\text{C} + ^{208}\text{Pb}$	5.82	3.91	6.69	2.46	2.33	3.21	3.94	4.51	2.54
$^{12}\text{C} + ^{28}\text{Si}$	6.11	3.04	2.05	2.47	2.32	2.83	2.09	1.36	2.93
$^{12}\text{C} + ^{90}\text{Zr}$	5.61	1.14	5.28	0.14	0.13	3.85	1.32	3.09	0.25
$^{12}\text{C} + ^{208}\text{Pb}$	5.04	2.38	4.67	1.45	1.64	4.32	1.75	2.93	1.45
$^{13}\text{C} + ^{12}\text{C}$	1014.3	40.6	81.4	43.0	159.4	632.4	100.9	151.4	49.6
$^{13}\text{C} + ^{28}\text{Si}$	12.3	5.84	6.18	6.19	5.65	7.89	6.72	6.20	5.92
$^{14}\text{C} + ^{13}\text{C}$	41.1	54.4	166.6	56.1	15.3	16.4	35.4	47.0	21.4
$^{14}\text{C} + ^{40}\text{Ca}$	4.71	1.00	6.10	0.32	0.25	4.86	1.33	1.17	0.29
$^{14}\text{C} + ^{138}\text{Ba}$	11.8	0.34	2.40	14.8	0.73	22.7	0.31	1.27	0.58
$^{15}\text{C} + ^{208}\text{Pb}$	4.54	4.50	4.51	4.94	4.94	4.94	4.94	4.50	4.94
$^{16}\text{C} + ^{12}\text{C}$	212.4	402.0	506.0	823.5	448.5	548.9	354.6	356.4	248.9

values compared to the other  $NN$  interactions in general.

In the present study, the results with eight different  $NN$  interactions have been compared with M3Y  $NN$  interaction potential in order to propose an alternative  $NN$  interaction. We have deduced that the SL and R3Y (HS)  $NN$  interactions would be an important alternative to M3Y  $NN$  interaction for the analysis of the elastic scattering cross-sections of carbon isotopes ( $^{10-16}\text{C}$ ).

## 5. Conclusions

We have investigated the effect of the B, G1, G2, SL, R3Y(HS), R3Y(Z), R3Y(W), R3Y(L1), and M3Y  $NN$  interaction potentials on the elastic scattering cross-sections of carbon isotopes by various target nuclei. We have observed that the reaction dynamics depend on the choice of  $NN$  interaction potential. In addition, we have noticed that the SL and R3Y (HS)  $NN$  interactions would be a good alternative to M3Y  $NN$  interaction. We think that it will be beneficial to apply these  $NN$  interactions simultaneously to inelastic scattering and transfer reactions.

1. G. Bertsch, J. Borysowich, A. McManus, W.G. Love. Interactions for inelastic scattering derived from realistic potentials. *Nucl. Phys. A* **284**, 399 (1977).
2. W.G. Greenless, G.J. Pyle, Y.C. Tang. Nuclear-matter radii from a reformulated optical model. *Phys. Rev.* **171**, 1115 (1968).
3. J.B. Ball, C.B. Fulmer, E.E. Gross, M.K. Halbert, D.C. Hensley, C.A. Ludemann, M.J. Saltmarsh, G.R. Satchler. Heavy ion elastic scattering survey: (I).  $^{208}\text{Pb}$  target. *Nucl. Phys. A* **252**, 208 (1975).
4. G.R. Satchler. *Direct Nuclear Reactions* (Oxford University Press, 1983).
5. C.J. Horowitz, B.D. Serot. Self-consistent hartree description of finite nuclei in a relativistic quantum field theory. *Nucl. Phys. A* **368**, 503 (1981).
6. P.G. Reinhard. The relativistic mean-field description of nuclei and nuclear dynamics. *Rep. Prog. Phys.* **52**, 439 (1989).
7. M. Kaur, A. Quddus, A. Kumar, M. Bhuyan, S.K. Patra. On the symmetry energy and deformed magic number at  $N = 100$  in rare earth nuclei. *J. Phys. G: Nucl. Part. Phys.* **47**, 105102 (2020).
8. B. Singh, M. Bhuyan, S.K. Patra, R.K. Gupta. Optical potential obtained from relativistic-mean-field theory-based microscopic nucleon-nucleon interaction: Applied to cluster radioactive decays. *J. Phys. G: Nucl. Part. Phys.* **39**, 025101 (2012).
9. B.B. Sahu, S.K. Singh, M. Bhuyan, S.K. Biswal, S.K. Patra. Importance of nonlinearity in the  $NN$  potential. *Phys. Rev. C* **89**, 034614 (2014).
10. M. Bhuyan, R. Kumar, S. Rana, D. Jain, S.K. Patra, B.V. Carlson. Effect of density and nucleon-nucleon potential on the fusion cross section within the relativistic mean field formalism. *Phys. Rev. C* **101**, 044603 (2020).
11. G.R. Satchler, W.G. Love. Folding model potentials from realistic interactions for heavy-ion scattering. *Phys. Rep.* **55**, 183 (1979).
12. R.K. Gupta, D. Singh, W. Greiner. Semiclassical and microscopic calculations of the spin-orbit density part of the Skyrme nucleus-nucleus interaction potential with temperature effects included. *Phys. Rev. C* **75**, 024603 (2007).
13. S. Hossain, M.N.A. Abdullah, Md.Z. Rahman, A.K Basak, F.B. Malik. Non-monotonic potentials for  $^6\text{Li}$  elastic scattering at 88 MeV. *Phys. Scr.* **87**, 015201 (2013).
14. M. El-Azab Farid, M.A. Hassanain. Density-independent folding analysis of the  $^{6,7}\text{Li}$  elastic scattering at intermediate energies. *Nucl. Phys. A* **678**, 39 (2000).
15. W. Zou, Y. Tian, Z.Yu Ma. Microscopic optical potential for  $\alpha$ -nucleus elastic scattering in a Dirac-Brueckner-Hartree-Fock approach. *Phys. Rev. C* **78**, 064613 (2008).
16. J. Cook. DFPOT – A program for the calculation of double folded potentials. *Commun. Comput. Phys.* **25**, 125 (1982).
17. I.J. Thompson. Coupled reaction channels calculations in nuclear physics. *Comput. Phys. Rep.* **7**, 167 (1988).
18. M. Aygun. Comprehensive research of  $^{10}\text{C}$  nucleus using different theoretical approaches. *Ukr. J. Phys.* **66**, 8 (2021).
19. M. Aygun. A comprehensive study on the internal structure and the density distribution of  $^{12}\text{Be}$ . *Rev. Mex. Fis.* **62**, 336 (2016).
20. M. Aygun. A microscopic analysis of elastic scattering of  $^8\text{Li}$  nucleus on different target nuclei. *Acta Phys. Pol. B* **45**, 1875 (2014).
21. S.Yu. Mezhevych, A.T. Rudchik, K. Rusek, K.W. Kemper, S. Kliczewski, E.I. Koshchy, A.A. Rudchik, S.B. Sakuta, J. Choiński, B. Czech, R. Siudak, A. Szczurek. Elastic and inelastic scattering of  $^{14}\text{C}+^{11}\text{B}$  versus  $^{12,13}\text{C} + ^{11}\text{B}$ . *Eur. Phys. J. A* **50**, 4 (2014).
22. J. Boguta, A.R. Bodmer. Relativistic calculation of nuclear matter and the nuclear surface. *Nucl. Phys. A* **292**, 413 (1977).
23. <http://nr.v.jinr.ru/nrv/>
24. J.D. Ovejas, A. Knyazev, I. Martel, O. Tengblad, M.J.G. Borge, J. Cederkall, N. Keeley, K. Rusek, C. García-Ramos, T. Pérez, L.A. Acosta, A.A. Arokiaraj, M. Babo, T. Cap, N. Ceylan and *et al.* Study of the scattering of  $^{15}\text{C}$  at energies around the Coulomb barrier. *J. Phys.: Conf. Ser.* **1643**, 012095 (2020).

Received 17.05.22

*M. Aygun*

АНАЛІЗ ПОПЕРЕЧНИХ  
ПЕРЕРІЗІВ ПРУЖНОГО РОЗСИЮВАННЯ  
ІЗОТОПІВ ( $^{10-16}\text{C}$ ) З ВИКОРИСТАННЯМ  
РІЗНИХ НУКЛОН-НУКЛОННИХ ВЗАЄМОДІЙ

В рамках оптичної моделі проведено порівняльний аналіз різних нуклон-нуклонних взаємодій. Отримано дійсний потенціал в моделі подвійної згортки (double folding model) для восьми різних нуклон-нуклонних взаємодій:  $V$ ,  $G1$ ,

$G2$ ,  $SL$ ,  $R3Y(HS)$ ,  $R3Y(Z)$ ,  $R3Y(W)$  та  $R3Y(L1)$ . Результати співставлено з отриманими для нуклон-нуклонної взаємодії  $M3Y$ , а також з експериментом. Обговорюються подібності та відмінності нуклон-нуклонних взаємодій і запропоновано їх альтернативні варіанти для дослідження ізотопів вуглецю ( $^{10-16}\text{C}$ ).

*Ключові слова:* нуклон-нуклонна взаємодія, релятивістичне середнє поле, оптична модель, модель подвійної згортки.